Journal of Macromolecular Science, Part A
Publication details, including instructions for authors and subscription information:
http://www.informaworld.com/smpp/title~content=t713597274

SYNTHESIS CHARACTERIZATION AND REMEDIATION POTENTIAL OF POLYMERIZABLE SURFACTANT MONOMERS OF *N,N*-DIALLYL-*N,N*-DIALKYL AMMONIUM CHLORIDE

Michael F. Richardson[a]; Charles L. McCormick[a]
[a] Department of Polymer Science, The University of Southern Mississippi, Hattiesburg, MS, U.S.A.

Online publication date: 20 September 1999

To cite this Article Richardson, Michael F. and McCormick, Charles L.(1999) 'SYNTHESIS CHARACTERIZATION AND REMEDIATION POTENTIAL OF POLYMERIZABLE SURFACTANT MONOMERS OF *N,N*-DIALLYL-*N,N*-DIALKYL AMMONIUM CHLORIDE', Journal of Macromolecular Science, Part A, 36: 10, 1349 — 1385
To link to this Article: DOI: 10.1081/MA-100101602
URL: http://dx.doi.org/10.1081/MA-100101602

J.M.S.—PURE APPL. CHEM., A36(10), pp. 1349–1385 (1999)

SYNTHESIS CHARACTERIZATION AND REMEDIATION POTENTIAL OF POLYMERIZABLE SURFACTANT MONOMERS OF *N*,*N*-DIALLYL-*N*,*N*-DIALKYL AMMONIUM CHLORIDE

Michael F. Richardson and Charles L. McCormick*

The University of Southern Mississippi
Department of Polymer Science
Southern Station Box 10076
Hattiesburg, MS 39406

Key Words: Polymerizable Surfactant, Cyclopolymerization, Hydrophobic Monomers, Remediation

ABSTRACT

The amphiphilic polymerizable surfactants *N*,*N*-diallyl-*N*,*N*-dioctylammonium chloride, *N*,*N*-diallyl-*N*,*N*-didecylammonium chloride and *N*,*N*-diallyl-*N*,*N*-didodecylammonium chloride have been synthesized. Experimental techniques including dynamic light scattering, fluorescence spectroscopy, nuclear magnetic resonance, and atomic force microscopy indicate the monomers form large, well-organized structures similar to vesicles of naturally occurring lipids. Studies of the sequestration of a model foulant by the didodecyl monomer revealed a strong interaction with a high degree of binding. The loading of higher amounts of cresol causes a change in the properties of the monomer assemblies indicating the formation of mixed micellar aggregates. The large monomer aggregates are retained by the dialysis membrane and present a potential alternative to small micellar assemblies.

* Author to whom correspondence should be addressed.

INTRODUCTION

Investigations of naturally occurring, organized structures have provided a new direction for scientists interested in the synthesis of specifically tailored materials. Preparation of stable synthetic analogs of lipid vesicles has led to new opportunities in several fields of research including synthetic membranes [1-9] energy conversion [10-14] and drug delivery [15-16] Twin tail surfactants that form organized vesicles have also been studied as remediation agents in waste-water treatment processes [17, 18].

Micellar enhanced ultrafiltration (MEUF) is a separation process utilized for the removal of organic compounds from water. In MEUF, surfactant is added to an aqueous solution containing the hydrophobic contaminant to be recovered. The micellar solution containing the foulant (retentate) is allowed to flow through a membrane that permits passage of water but prevents passage of the foulant-loaded surfactant micelles. A limitation of small molecule surfactants in MEUF is the passage of individual surfactant molecules through the membrane into the permeate [19]. These surfactants are often considered pollutants and must be minimized for MEUF processes to gain wide acceptance. The use of twin tail surfactants that form vesicles in solution may lead to improvements in MEUF. The large size of the structures and their inherent stability limit passage across the membrane into the permeate. Such vesicles should allow the use of membranes with a larger pore size, resulting in a higher flux of permeate [19].

In this paper, we report the synthesis and characterization of the monomers of diallyldioctylammonium chloride, diallyldidecylammonium chloride and diallyldidodecylammonium chloride. The effects of concentration of monomer were studied with surface tension, fluorescence, classical light scattering, dynamic light scattering, nuclear magnetic resonance, atomic force microscopy, polarizing microscopy and small angle X-ray scattering. The sequestration of *p*-cresol by the twin tail C_{12} monomer was investigated with equilibrium dialysis. The monomer was found to exhibit a strong interaction with *p*-cresol and appears to form mixed micelles at high loading of *p*-cresol.

EXPERIMENTAL

Materials

Diallylamine, 1-bromooctane, 1-bromodecane and 1-bromododecane were purchased from Aldrich Chemical Company. Each reagent was distilled

under vacuum (5 mm Hg) twice prior to use. Pyrene and *p*-cresol were purchased from Aldrich Chemical Company (Milwaukee, WI). Para-cresol was purified by vacuum distillation. Water used in the studies was deionized and possessed a conductance $<10^{-7}$ mho/cm. Water used for surface measurements was double distilled from a permanganate solution and had a surface tension of 72 mN/m. Other reagents and materials were purchased commercially and used as received.

Monomer Synthesis

Single Tail Monomers, N,N-Diallyl-N-Octylamine (1), N,N-Diallyl-N-Decylamine (2) N,N-Diallyl-N-Dodecylamine (3)

The scheme for synthesis of the single tail monomers is illustrated in Scheme 1. Diallylamine (242.9 g 2.5 mol) was added to 200 ml of toluene in a three-neck round-bottomed flask (1 l). 1-Bromooctane (386.26 g, 2.0 mol), 1-bromodecane (373.8 g, 1.5 mol) or 1-bromododecane (382.3 g, 1.97 mol) was then added to this solution and heated to reflux for 24 hours. One hour after the start of the reaction, an orange or brown solid (depending on the bromoalkane) was observed at the top of the solution. After three hours, the solid had dissolved and the entire solution became a dark brown color. After cooling the solution, 200 ml of distilled water was added and the pH was adjusted to 10.0 with a concentrated sodium hydroxide solution. The dispersion was extracted three times with 300 ml of diethyl ether. The ether phase was collected and dried with potassium carbonate. The ether was removed on a rotary evaporator. The dried solution was distilled under atmospheric pressure to remove residual ether and toluene. The final products (95%) were collected under vacuum (5 mm Hg) at 80-88°C (1), 138°C (2) and 170°C (3) as colorless oils. Analysis for (1) - ^{1}H

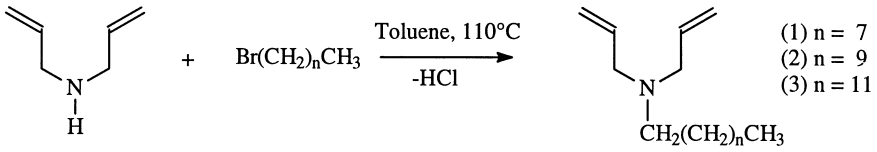

Scheme 1. Synthesis of *N*,*N*-diallyl-*N*-alkylamines (1), (2), (3).

NMR ($CDCl_3$) δ (ppm) 0.89 (s, 3H), 1.29-1.45 (m, 12H), 2.40 (t, 2H), 3.05 (d, 4H), 5.13 (m, 4H), 5.83 (m, 2H). ^{13}C NMR ($CDCl_3$) δ (ppm) 14.3, 23.1, 27.8, 29.4, 31.1, 53.6, 57.0, 117.2, 136.7. FTIR 3080 (C=C-H), 2924 (aliphatic C-H stretch), 1645 (C=C), 1456 (C-H Bend) Elemental Analysis (theory/found) %C (80.4/80.5) %H (12.9/13.0) %N (6.7/6.6). Analysis for (2) - ^1H NMR ($CDCl_3$) δ (ppm) 0.89 (t, 3H), 1.29-1.45 (m, 14H), 2.40 (t, 2H), 3.07 (d, 4H), 5.13 (m, 4H), 5.84 (m, 2H). ^{13}C NMR ($CDCl_3$) δ (ppm) 14.3, 22.8, 27.4, 29.7, 32.0, 55.5, 57.0, 117.0, 136.1. FTIR 3080 (C=C-H), 2924 (aliphatic C-H stretch), 1645 (C=C), 1456 (C-H Bend) Elemental Analysis (theory/found) %C (81.0/80.9) %H (13.0/13.0) %N (5.9/5.8). Analysis for (3) - ^1H NMR ($CDCl_3$) δ (ppm) 0.87 (t, 3H), 1.29-1.45 (m, 18H), 2.42 (t, 2H), 3.09 (d, 4H), 5.12 (m, 4H), 5.84 (m, 2H). ^{13}C NMR ($CDCl_3$) δ (ppm) 14.2, 22.8, 27.4, 29.7, 31.9, 53.2, 56.9, 116.7, 136.1. FTIR 3080 (C=C-H), 2924 (aliphatic C-H stretch), 1645 (C=C), 1456 (C-H Bend) Elemental Analysis (theory/found) %C (81.5/81.2) %H (13.2/13.2) %N (5.3/5.1).

Twin Tail Monomers, N,N-Diallyl-N,N-Dioctylammonium Chloride (4). N,N-Diallyl-N,N-Didecylammonium Chloride (5), N,N-Diallyl-N,N-Didodecylammonium Chloride (6)

The synthetic route for the twin tail monomers is illustrated in Scheme 2. *N,N*-diallyl-*N*-alkylamine (1), (2), or (3) (1.5 mol) and the corresponding 1-bromoalkane (2.0 mol) were placed in 150 ml of acetonitrile in a round bottomed flask. The solution was heated to reflux for four days. The acetonitrile was removed on a rotary evaporator. The resulting light brown oil was extracted three times with 300 ml of hexane followed by three extractions with 300 ml of diethyl ether. The resulting product was dried under vacuum to remove residual solvent. Excessive foaming of the oil phase was observed and was controlled

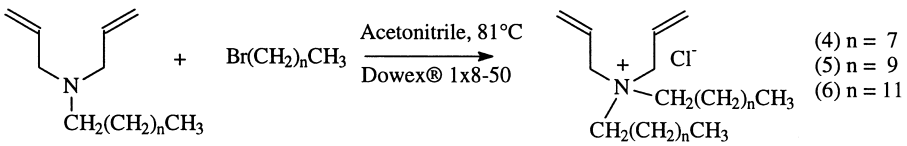

Scheme 2. Synthesis of *N,N*-diallyl-*N,N*-dialkyl ammonium chlorides (4), (5), (6).

with regulation of the vacuum. The final product was a slightly yellow oil (~95%). The counterion was converted to the chloride using Dowex® 1X8-50 (Cl^-) ion exchange resin. Analysis for (4) - ^{1}H NMR ($CDCl_3$) δ (ppm) 0.88 (s, 6H), 1.28-1.34 (m, 20H), 1.83 (s, 4H), 3.37 (s, 4H), 4.21 (s, 4H), 5.71-5.85 (m, 4H), 6.10 (m, 2H). ^{13}C NMR ($CDCl_3$) δ (ppm) 14.2, 22.5, 26.6, 29.1, 31.6, 59.2, 61.6, 124.3, 128.9 FTIR 3080 (C=C-H), 2860 (aliphatic C-H stretch), 1650 (C=C), 1467 (C-H Bend), 1377 (CH_3) Elemental Analysis (theory/found) %C (65.6/66.8) %H (10.9/10.7) %N (3.4/3.1). Analysis for (5) - ^{1}H NMR ($CDCl_3$) δ (ppm) 0.91 (s, 6H), 1.30-1.34 (s, 28H), 1.85 (s, 4H), 3.39 (s, 4H), 4.23 (s, 4H), 5.73-5.90 (m, 4H), 6.11 (s, 2H). ^{13}C NMR ($CDCl_3$) δ (ppm) 14.2, 22.6, 26.6, 29.3, 31.8, 59.0, 61.6, 124.7, 128.7. FTIR 3080 (C=C-H), 2860 (aliphatic C-H stretch), 1650 (C=C), 1467 (C-H Bend), 1377 (CH_3) Elemental Analysis (theory/found) %C (68.1/65.1) %H (11.4/10.3) %N (3.1/3.5). Analysis for (6) - ^{1}H NMR ($CDCl_3$) δ (ppm) 0.88 (s, 6H), 1.27 (s, 36H), 1.80 (s, 4H), 3.34 (s, 4H), 4.22 (s, 4H), 5.72-5.83 (m, 4H), 6.10 (m, 2H). ^{13}C NMR ($CDCl_3$) δ (ppm) 14.3, 22.6, 26.8, 29.53, 31.9, 59.2, 61.7, 124.6, 129.1. FTIR 3080 (C=C-H), 2860 (aliphatic C-H stretch), 1650 (C=C), 1467 (C-H Bend), 1377 (CH_3) Elemental Analysis (theory/found) %C (70.0/69.8) %H (11.7/11.6) %N (2.7/2.5).

Characterization Methods

^{1}H and ^{13}C NMR spectra were recorded with a Bruker AC-300. Infrared spectra were measured with a Nicolet 460 FT-IR spectrometer. Barium fluoride plates used for obtaining the sample spectrum allowed spectral monitoring from 4000 cm^{-1} to 870 cm^{-1}. A spectral resolution of 4 cm^{-1} was employed. Elemental analyses were performed by M-H-W laboratories of Phoenix AZ. Carbon, hydrogen and nitrogen analyses were performed with a reported accuracy of 0.02%. Classical and dynamic light scattering measurements were made with a Brookhaven Instruments 128-channel BI-2030 AT digital correlator using a Spectra Physics He-Ne Laser operating at 632.8 nm. The collected autocorrelation functions were analyzed using the methods of cumulants and/or CONTIN [20]. Samples were clarified for light scattering measurements by centrifugation. UV-vis measurements were made with a Hewlett-Packard 8452A diode array spectrophotometer. Fluorescence emission spectra were measured at 25°C with an Edinburgh Instruments FS900CDT T-Geometry fluorometer. Equilibrium surface tensions were taken on a Kruss™ K12 Tensiometer using the Wilhelmy plate method. Surface tension versus concentration profiles were obtained so that each data point reflects an average of five consecutive measurements whose

standard deviation was < 0.002mN/M. All glassware for surface tension measurements was cleaned by soaking in nitric acid for > 2 hours, followed by rinsing with surface water repeatedly. The platinum plate was cleaned by flaming. Measurements varied from approximately two hours to two days. Concentrations for the critical aggregation concentration, (CAC), were taken at the minimum of the impurity well or extrapolated, (depending on the data profile), for curves which yielded an unclear break in the slope. AFM images were obtained with a Multi-Mode Nanoscope III Microscope (Digital Instruments) using the Tapping Mode. SAXS data were collected using a Siemens XPD-700P polymer diffraction system equipped with a two-dimensional, position-sensitive area detector. A Nikon Optiphot2 polarizing optical microscope was used for determining the optical birefringence of liquid crystalline samples. Equilibrium dialysis experiments were performed utilizing dialysis cells (5 ml) from Bel-Art Products and regenerated cellulose membranes having a nominal molecular weight cutoff of 6000. Temperature dependent studies were performed at 5°C in a water bath regulated with a Lauda RM6 water circulator and at 25°C and 45°C in a Napco incubator.

Equilibrium Dialysis Data Analysis

Classical remediation models consider the micelle as a distinct pseudophase containing the hydrophobic foulant [28]. For small amphipathic molecules, micelles form only above a critical concentration, termed the critical micelle concentration (CMC). In some cases, the foulant is considered a "guest" within the micelle, while in others it participates in forming mixed micelles. If the monomer aggregates are treated as discrete solubilizing entities, then it is possible to propose a series of expressions that define the interaction between the foulant and the monomer aggregates. The concentration of the foulant in the aggregate is determined from the concentration of the foulant in the retentate ($[foulant]_{ret}$) and in the permeate ($[foulant]_{per}$) via Equation 1:

$$[foulant]_{bnd} = [foulant]_{ret} - [foulant]_{per} \quad (1)$$

Equation 1 remains valid if the concentration of foulant in the permeate is equivalent to the concentration of unbound foulant in the retentate. With knowledge of the amount of foulant bound within the hydrophobic microdomains the molar binding ratio, *r*, can be determined utilizing Equation 2.

$$r = \frac{[foulant]_{bnd}}{[monomer]} \tag{2}$$

in which [*monomer*] is the concentration of the monomer in the retentate. Binding isotherms may be constructed by plotting *r* as a function of the feed foulant concentration.

Knowledge of the concentration of the foulant in each compartment of the dialysis cell at the conclusion of the experiment, combined with knowledge of the monomer concentration in the retentate compartment, also allows calculation of the equilibrium constant *k* as illustrated in Equation 3.

$$k = \frac{[foulant]_{retentate} - [foulant]_{permeate}}{[foulant]_{permeate} \cdot [monomer]} \tag{3}$$

The term *k* is simply a mass action equilibrium constant for the transfer of the foulant from the aqueous 'bulk' phase to the hydrophobic microdomain. This ratio has been used extensively in the literature, but it is more convenient to use an alternate equilibrium constant K, defined by Equation 4 [21-27].

$$K = \frac{X}{c_0} \tag{4}$$

where X represents the mole fraction of the organic solute in the monomer domain and c_0 represents the concentration of free foulant present in a non-associated state [28] The two equilibrium constants *k* and K are easily determined from the experimental data and are related by Equation 5 [29].

$$K = k(1 - X) \tag{5}$$

An advantage of using the equilibrium constant K is that it has been shown to be closely related to the activity coefficient of the foulant in the domain [29]. This activity coefficient may be calculated using Equation 6.

$$K = \frac{1}{\gamma_0 c_0^0} \tag{6}$$

where γ_0 is the activity coefficient of the foulant and c_0^0 is the saturation concentration of the foulant in water (0.18 M) [30]. The value is simply interpreted as a measure of the escaping tendency of the foulant from the domain. Information regarding the activity coefficient and the variance of γ_0 with X is useful in defining the environment of the foulant within the domain.

The overall efficiency of foulant sequestration may be evaluated from the rejection ratio. While the binding isotherms and activity coefficients reflect the interaction of the monomer with the foulant on a molecular basis, the rejection ratio provides a practical means of determining effectiveness for remediation of the foulant from an aqueous wastewater stream. The value of the rejection ratio is calculated from the equilibrium dialysis data and is defined by Equation 7. Thus the rejection ratio is a measure of how well the monomer prevents passage of the foulant through the membrane. Low values indicate that the monomer has a low capacity for capture. High rejection ratios indicate that the monomer domain is capable of interacting with and retaining the foulant.

$$\text{Rejection Ratio} = \left(1 - \frac{[Cresol]_{per}}{[Cresol]_{ret}}\right) \times 100 \tag{7}$$

RESULTS AND DISCUSSION

This section details the synthesis and characterization of a series of assoiative polymerizable surfactants. The objective of this research was the synthesis of self-ordering amphiphilic molecules that would form highly organized microphase domains useful in remediation via MEUF processes. Here, amphiphilic surfactant molecules, similar in structure to naturally occurring lipids, were synthesized. The phase behavior was studied to determine the concentration dependence and properties of the domains formed by the surfactants. Finally, interaction of the surfactants with *p*-cresol was studied using equilibrium dialysis experiments.

Monomer Synthesis and Structural Characterization

A primary objective of this work is the synthesis of a series of single and twin tailed surfactants with alkyl chain lengths of eight, ten and twelve carbons (Figure 13). The monomers were prepared utilizing the synthetic procedures shown in Schemes 1 and 2. This procedure afforded both the single and twin tail

surfactants. Isolation of the single tail monomers was straightforward using vacuum distillation. The purification of the twin tail monomers was hindered by isolation of the quaternary amine following the addition of the second alkyl tail. The monomers could be recrystallized from cold ethyl acetate; however, the recovery of the monomers was limited due to rapid melting of the solid and resolubilization in the ethyl acetate. The most direct means for purification of the monomers was by of a series of solvent extractions. Three extractions with hexane followed by three extractions with diethyl ether were necessary to purify the monomers. The solvent was removed under vacuum over a period of days at room temperature. Analysis of the single tail and twin tail monomer products was accomplished utilizing NMR, FT-IR and elemental analysis (Figures 1-13).

Monomer Solution Behavior

Prior to the study of the solution properties of the polymerizable surfactants, predictions of the aqueous solution behavior were gained by examination of literature reports of surfactants with similar chemical structure [31-40]. For example, several groups have examined the relationship between surfactant structural geometry and aggregate shape and size [41-43]. The research has shown that aggregate formation in solution is driven by the free energies of the systems. For surfactants, this free energy arises from the interplay of chain packing of hydrophobic tails and the repulsions among polar or ionic head-groups. As a result, a wide range of structures has been observed. Micelles, oblate

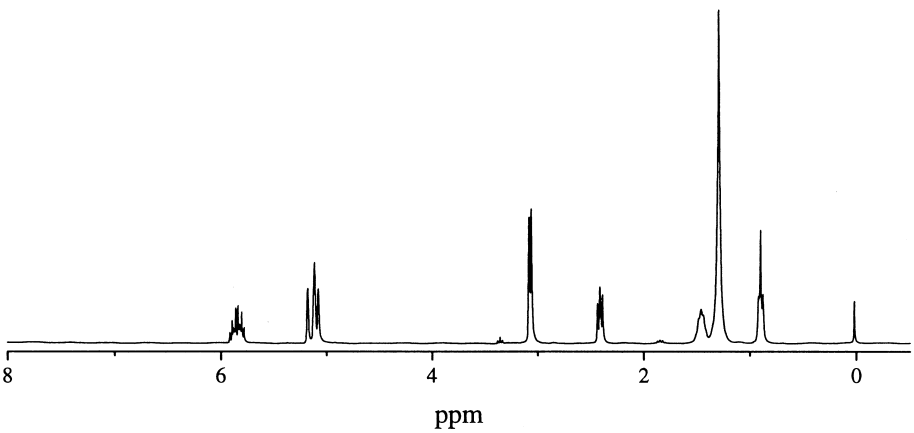

Figure 1. ^{1}H NMR of *N*,*N*-diallyl-*N*-octylamine ($CDCl_3$).

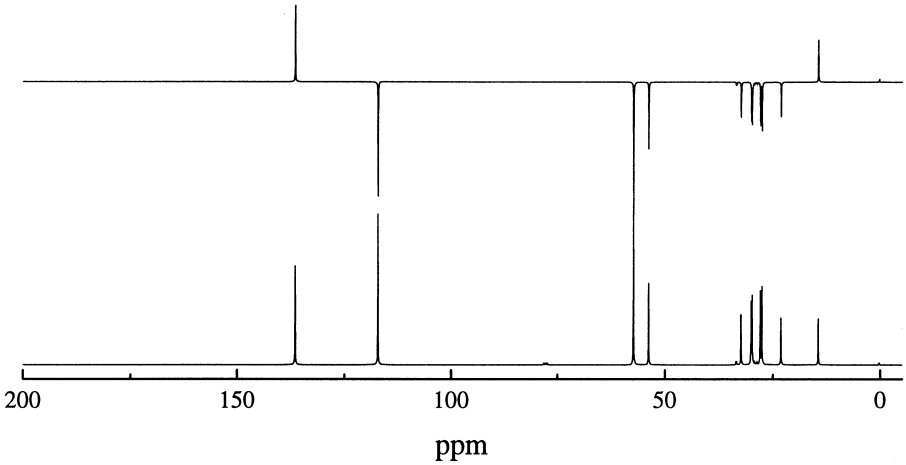

Figure 2. ^{13}C NMR (bottom) and DEPT 135 (top) of *N*,*N*-diallyl-*N*-octylamine ($CDCl_3$).

micelles, unilamellar bilayers, multilamellar bilayers and inverse structures can be obtained depending on the nature of the headgroups and the dimensions of the hydrophobic tails.

Statistical mechanics provides a means for predicting the shapes of surfactant aggregates. The surfactant parameter defined as *v/al*, has been used extensively to predict the structure of numerous surfactant [41]. Each of the

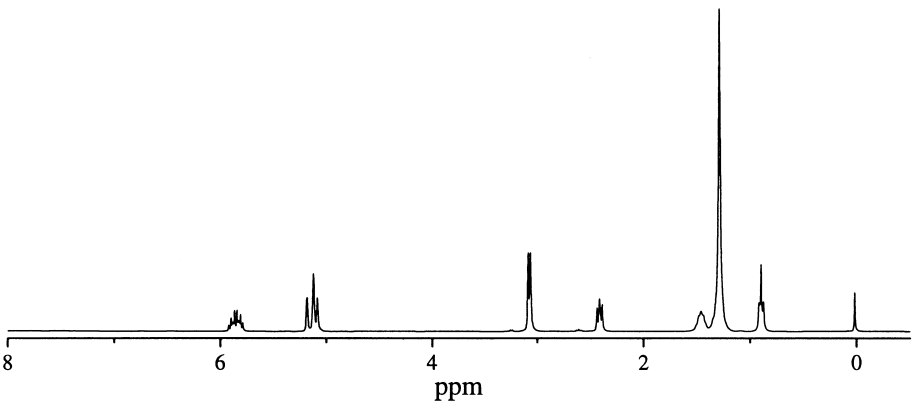

Figure 3. ^{1}H NMR of *N*,*N*-diallyl-*N*-decylamine ($CDCl_3$).

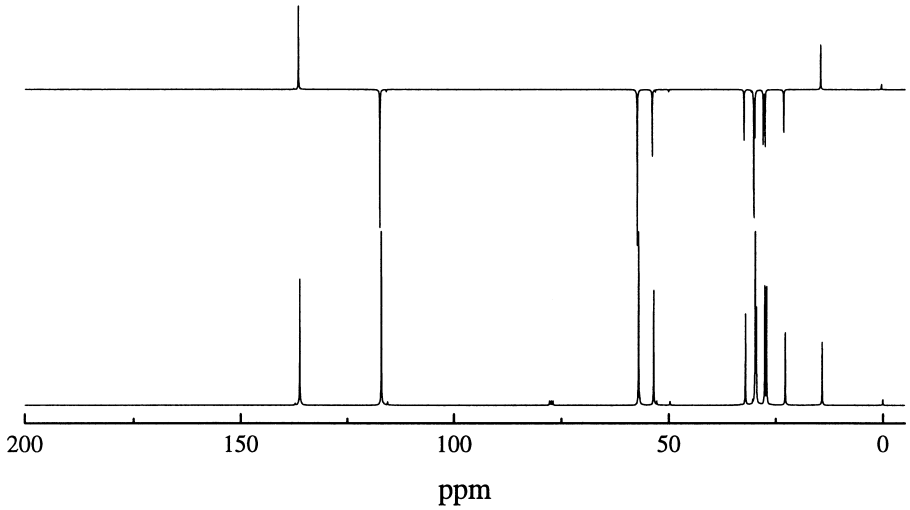

Figure 4. ^{13}C NMR (bottom) and DEPT 135 (top) of *N*,*N*-diallyl-*N*-decylamine ($CDCl_3$).

terms of the surfactant parameter is related to a structural property of the surfactant (Figure 14). The term *v* is the volume of the hydrocarbon chain of the surfactant, *l* is the length of the fully extended hydrocarbon chain, and *a* is the head group area. Spherical micelles are predicted for surfactants with $v/al < 1/3$. Cylindrical micelles are anticipated for surfactants with $1/3 < v/al < 1/2$. Vesicles or oblate micelles are expected at $1/2 < v/al < 1$. Based on dimensions

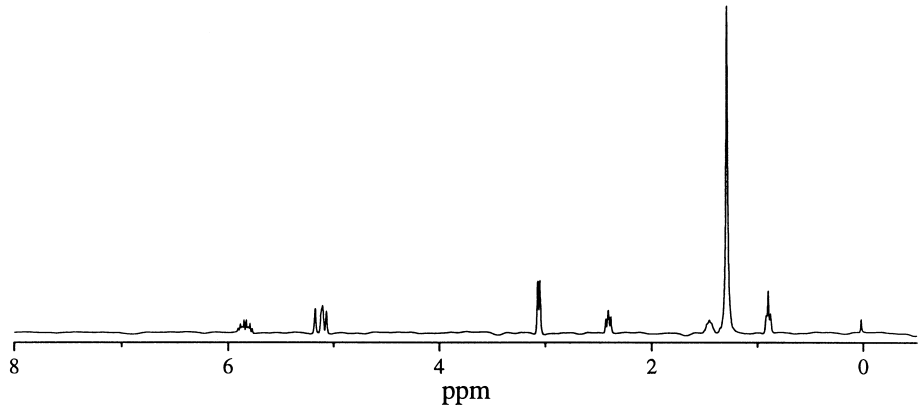

Figure 5. ^{1}H NMR of *N*,*N*-diallyl-*N*-dodecylamine ($CDCl_3$).

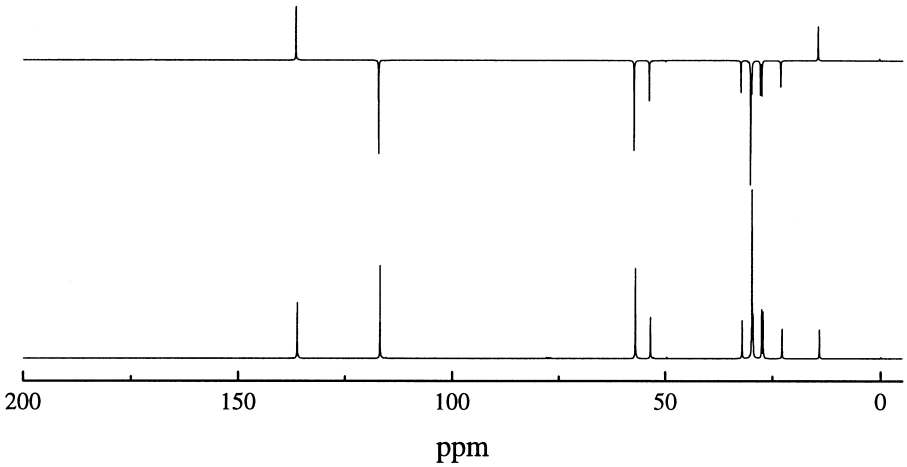

Figure 6. ^{13}C NMR (bottom) and DEPT 135 (top) of *N*,*N*-diallyl-*N*-dodecylamine ($CDCl_3$).

previously published for surfactants of similar chemical composition [31], the values for the surfactant parameter were calculated for each of the monomers synthesized (see Table 1). The value calculated for each of the single tail surfactants was 0.2. According to the theory, the aggregates formed by the surfactants would be small, spherical micelles, similar to other small molecule surfactants such as cetyltrimethylammonium bromide (CTAB). CTAB has a surfactant

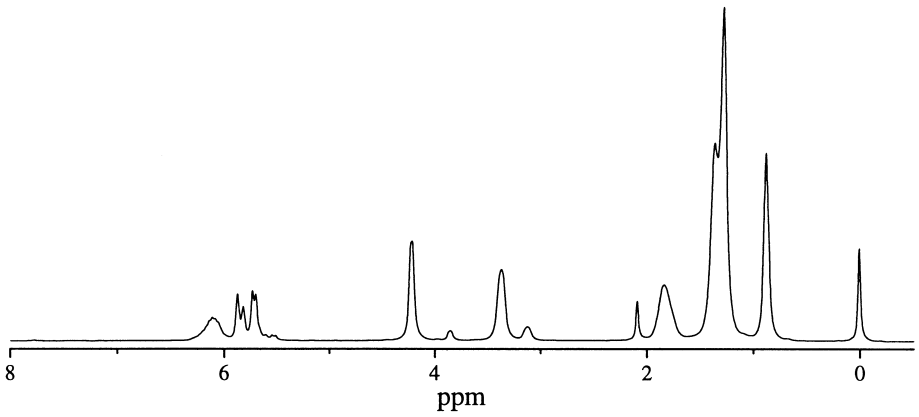

Figure 7. ^{1}H NMR of *N*,*N*-diallyl-*N*,*N*-dioctylammonium chloride ($CDCl_3$).

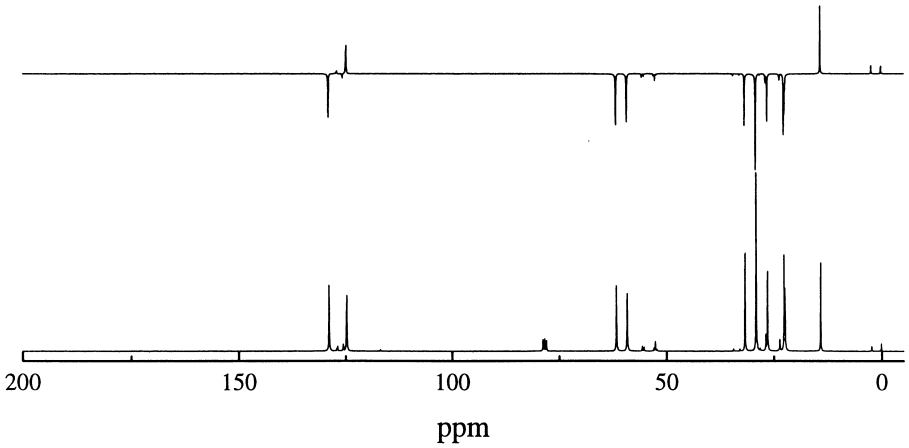

Figure 8. ^{13}C NMR (bottom) and DEPT 135 (top) of *N*,*N*-diallyl-*N*,*N*-dioctylammonium chloride ($CDCl_3$).

parameter value of 0.33 and is widely known to form spherical micelles at low concentrations [44]. The value for each of the polymerizable twin tail surfactants is approximately 0.80. Based on the theory, these surfactants should form vesicles, oblate micelles or bilayers depending on the concentration.

In an effort to further define the anticipated solution behavior of the twin tail surfactant monomers, the previously documented phase behaviors of the related didodecyldimethylammonium chloride (DDAC) and bromide (DDAB)

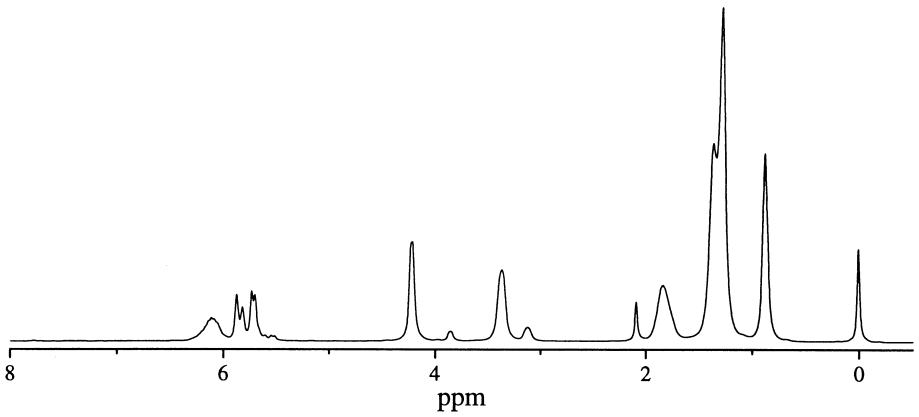

Figure 9. ^{1}H NMR of *N*,*N*-Diallyl-*N*,*N*-didecylammonium chloride ($CDCl_3$).

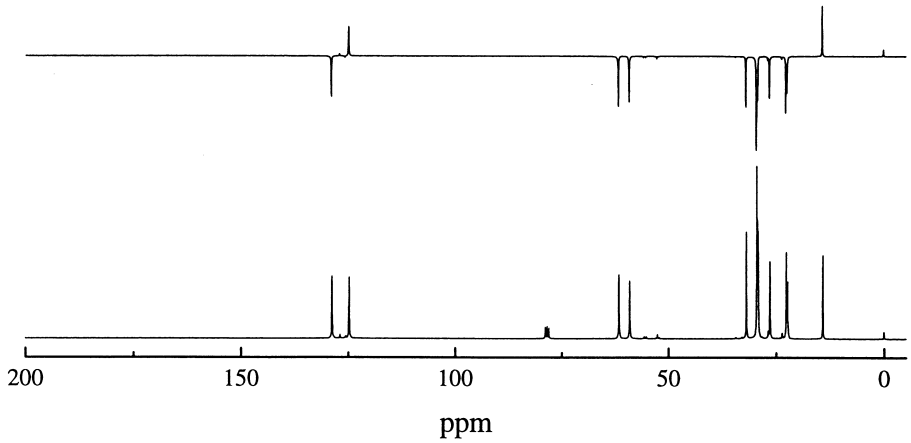

Figure 10. ^{13}C NMR (bottom) and DEPT 135 (top) of *N*,*N*-diallyl-*N*,*N*-didecylammonium chloride ($CDCl_3$).

were studied (Figure 15) [33, 38]. The primary characteristic that distinguishes the C_{12} twin tail monomer and the model surfactants is the replacement of the twin methyl groups of the quaternary amine surfactant with the twin allyl groups of the monomer. Characterization of DDAB with surface tension indicates a critical aggregation concentration of approximately $4x10^{-5}$M [44]. Above this concentration, the surfactant forms multilamellar vesicles [33]. At higher concen-

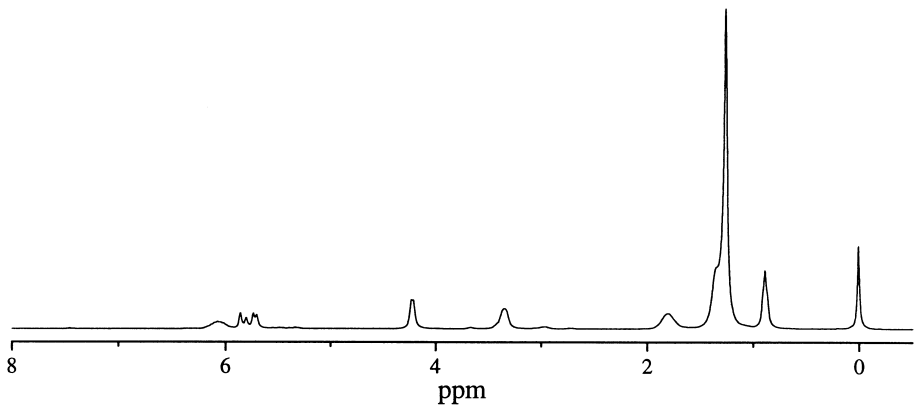

Figure 11. ^{1}H NMR of *N*,*N*-diallyl-*N*,*N*-didodecylammonium chloride ($CDCl_3$).

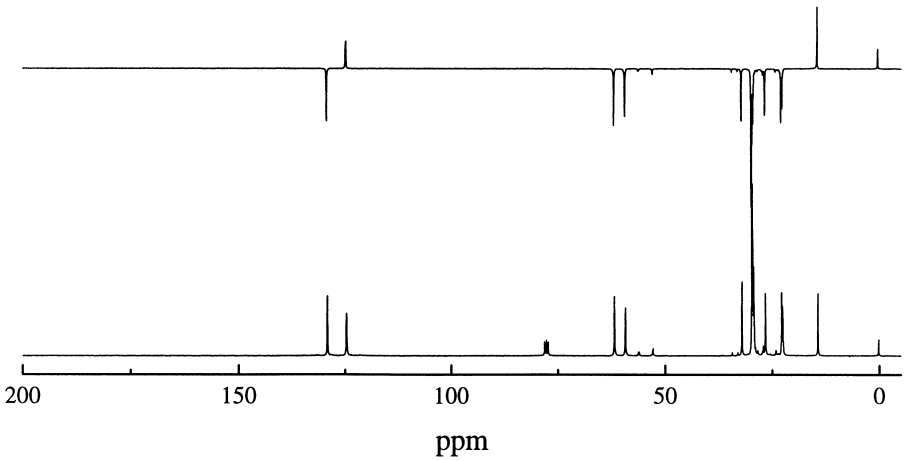

Figure 12. ^{13}C NMR (bottom) and DEPT 135 (top) of *N*,*N*-diallyl-*N*,*N*-didodecylammonium chloride ($CDCl_3$).

trations of surfactant, liquid crystalline properties are observed with polarizing microscopy and deuterium NMR [33]. DDAC possesses a lamellar phase in water from 18-88 wt% surfactant. Other phases, such as hexagonal or cubic were not observed with DDAC. The solution behavior of DDAC and DDAB closely match that predicted by the calculations of the surfactant parameter. Utilizing information from the structurally similar model compound, the twin tail monomers are expected to form vesicles at low concentrations, followed by liquid crystalline lamellar phases at higher concentrations.

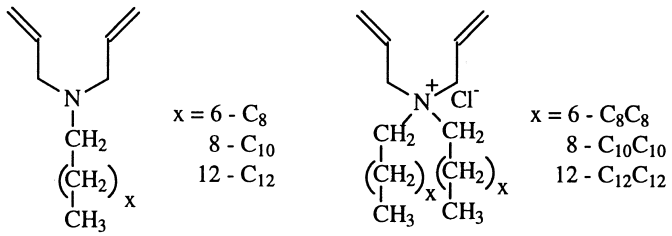

Figure 13. Single and twin tail monomers based on diallylamine.

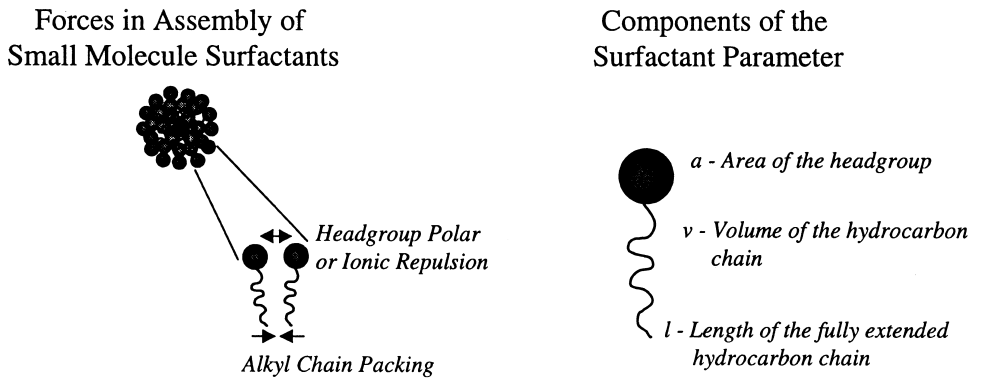

Figure 14. Forces in surfactant assembly and the components of the surfactant parameter governing the size and shape of surfactant assemblies.

Potentiometric Titration

Prior to surface tension measurements of the single tail surfactants, the pKa values of the tertiary amine of the monomers were determined by potentiometric titrations (Figure 16). The pKa values measured for each of the monomers decrease with the length of the alkyl chains. This decrease is attributed to an increase in the hydrophobicity of the surfactant monomers. As acid is added to a solution of the neutralized monomers, a certain percentage of the ter-

TABLE 1. Values of the Components of the Surfactant Parameter and the Calculated Surfactant Parameter for Each of the Synthetic Monomers

Monomer	v (Å^3)[c]	a (Å^2)[b]	l (Å)[a]	v/al
C_8 Single Tail	121	52	11.6	0.20
C_{10} Single Tail	147	52	14.1	0.20
C_{12} Single Tail	173	52	16.6	0.20
C_8 Twin Tail	485	52	11.6	0.80
C_{10} Twin Tail	593	52	14.1	0.80
C_{12} Twin Tail	700	52	16.6	0.81

[a]Length of the alkyl chain determined from Tanford's formula, $l = 1.50 + 1.265$(no. carbons)[59]

[b]Area of the headgroup determined from the work of Ninham et. al.[37]

[c]Volume of the alkyl chains determined from Gruen's equation, v=54.3(no. CH_3)+27.0(no. CH_2)[60]

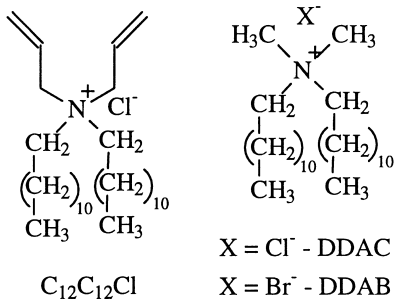

Figure 15. Structures of twin tail $C_{12}C_{12}$ monomer and didodecyldimethylammonium chloride (DDAC).

tiary amine groups are protonated. With increasing acid concentration, the population of surface active monomers increases. Above a certain pH, the population of surface active monomers is above a critical micelle concentration. The uncharged (unprotonated) monomer likely participates to create mixed micelles. The micelles formed by surfactants with longer alkyl chains are more hydrophobic. As a result, ionization of the remaining monomers in the mixed micelle is

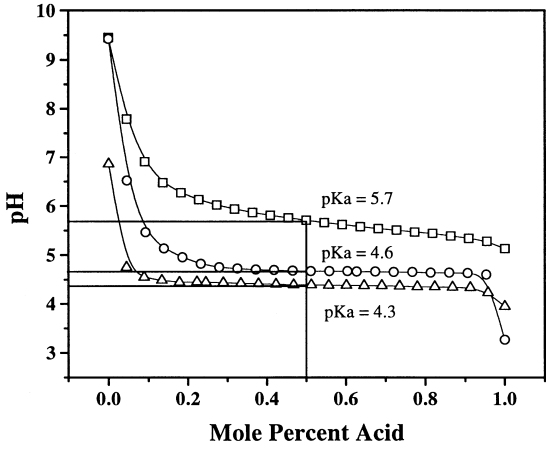

Figure 16. Potentiometric titrations for single tail *N*,*N*-diallyl-*N*-alkyl ammonium chlorides. (□) - *N*,*N*-diallyl-*N*-octyl ammonium chloride, (○) - *N*,*N*-diallyl-*N*-decyl ammonium chloride, (Δ) - *N*,*N*-diallyl-*N*-dodecyl ammonium chloride.

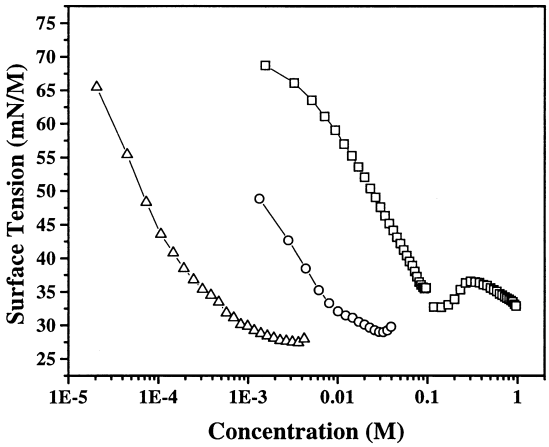

Figure 17. Surface tension as a function of concentration of monomer for single tail *N*,*N*-diallyl-*N*-alkyl ammonium chlorides. (□) *N*,*N*-diallyl-*N*-octyl ammonium chloride (○) *N*,*N*-diallyl-*N*-decyl ammonium chloride, (Δ) *N*,*N*-diallyl-*N*-dodecyl ammonium chloride. pH = 2.0, T = 25°C.

suppressed requiring higher concentrations of acid. This shielding of the uncharged monomers in the mixed micelle leads to a lower observed value of the pKa.

Once the pKa values were determined for the single tail monomers, the surface activities of the monomers in water were studied via surface tension measurements at pH 2.0. Figure 17 illustrates the changes in surface tension of water with the concentration for single tail monomers. As the concentration of monomer in solution increases, the surface tension of the solution decreases. Extrapolations of the linear regions of the surface tension plots indicate the critical micelle concentration for each of the monomers (Table 2). The CMC for each monomer changes with the length of the hydrophobic alkyl chain. The CMC for the octyl monomer occurs at a concentration higher than those for the decyl and dodecyl monomers.

The surface activities of the twin tail surfactant molecules were also studied utilizing surface tension measurements. The results of the experiments are illustrated in Figure 18. As with the single tail monomers, the characteristic changes in slope are attributed to the formation of surfactant aggregates in solution. Extrapolations of the linear regions of the plot of the surface tension mea-

TABLE 2. Solution Properties of Single and Twin Tail Monomers

Monomer	CMC or CAC (M)[a]	CAC (M)[b]	Hydrodynamic Diameter (nm)
C_8	0.2	-	-
C_{10}	0.02	-	-
C_{12}	$2.5x10^{-3}$	-	-
C_8C_8	$2.0x10^{-5}$	$2.8x10^{-5}$	184±5 [c]
$C_{10}C_{10}$	$4.8x10^{-5}$	$2.0x10^{-4}$	150±4 [d]
$C_{12}C_{12}$	$3.8x10^{-6}$	$1.0x10^{-5}$	163±3 [c]

[a] Determined from surface tension
[b] Determined from light Scattering
[c] Monomer concentration .01 g dL^{-1}
[d] Monomer concentration .1 g dL^{-1}

surements provide the critical aggregation concentration (CAC) for each of the monomers (Table 2). As expected, the CAC for the twin tail monomers depends on the alkyl chain length. For each twin tail monomer, a broad maximum in the surface tension profile is observed at concentrations slightly above the CAC. This feature in surface tension measurements is often attributed to a packing rearrangement among the surfactants [45]. At higher concentrations, the surface tension values reach a constant value illustrating no further changes at the surface.

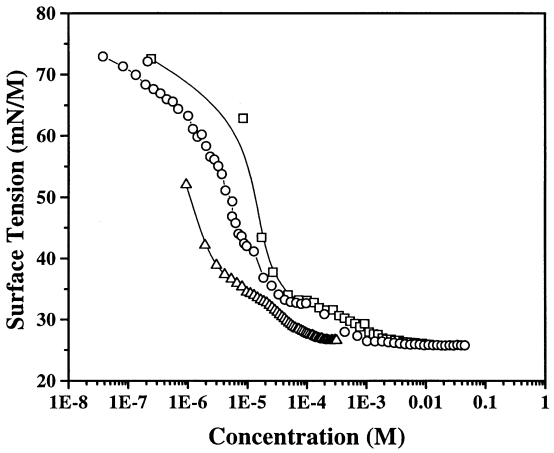

Figure 18. Surface tension as a function of concentration of monomer for twin tail *N*,*N*-diallyl-*N*,*N*-dialkyl ammonium chlorides. (□) *N*,*N*-diallyl-*N*,*N*-dioctyl ammonium chloride, (○) *N*,*N*-diallyl-*N*,*N*-didecyl ammonium chloride, (Δ) *N*,*N*-diallyl-*N*,*N*-didodecyl ammonium chloride.

To study the nature of the aggregates formed at concentrations above the CAC, light scattering measurements were performed. First, the intensity of light scattered at 90° was measured at a range of concentrations. As with the surface tension measurements, a critical concentration is observed in the light scattering profiles. Below the critical concentration, only low scattering intensities are observed. Near the CAC determined with surface tension, a distinct increase in scattering intensity is seen. The scattering profiles for the twin tail monomers are illustrated in Figure 19.

The increase in the scattering intensity observed with each of the twin tail monomers is attributed to the formation of large aggregates of the monomer. Dynamic light scattering measurements were performed to determine the size of the aggregates. Solutions of the monomer at concentrations above the observed CAC were prepared for each of the twin tail monomers. The values of the hydrodynamic diameter of each monomer at 1 mg/l are listed in Table 2. The monomers associate in solution to form structures with hydrodynamic diameters in excess of 150 nm. The size of the aggregates suggests the presence of a highly ordered microstructure much larger than classical surfactant micelles.

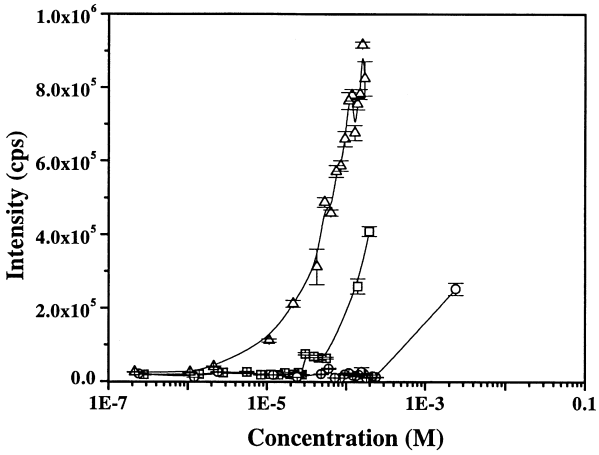

Figure 19. Light scattering intensity as a function of monomer concentration. (□) N,N-diallyl-N,N-dioctyl ammonium chloride, (○) N,N-diallyl-N,N-didecyl ammonium chloride, (Δ) N,N-diallyl-N,N-didodecyl ammonium chloride.

The influence of salt on the aggregation of the monomers was studied at a monomer concentration of 1×10^{-2}M. Incremental additions of NaCl were made to solutions of monomers and the corresponding autocorrelation functions were analyzed. A critical salt concentration is reached at 0.01 M NaCl. Above this concentration, the hydrodynamic diameter increases rapidly from ~150 nm to values in excess of 1 μm. The concentration of 0.01 M corresponds to a 1:1 ratio of added salt to monomer. The increase in the hydrodynamic diameter is attributed to the shielding of the ionic charges of the monomer head groups. Reducing the headgroup size causes a change in the packing of the surfactant molecules. A smaller headgroup causes the surfactants to have a more cylindrical shape, which would favor the formation of large, extended lamellar structures.

Fluorescence Spectroscopy

Fluorescence studies were conducted to investigate the solution properties of the aggregates of the twin tail monomers. Pyrene fluorescence measurements were performed to follow the changes in the polarity of the local environment of the pyrene molecule with increasing monomer concentration. The ratio of the first to the third emission bands of pyrene is a commonly used as a measure of the polarity of the microenvironment immediately around the fluorescent probe [46]. The results of pyrene fluorescence measurements with increasing didecyl monomer concentration are illustrated in Figure 20. The I_1/I_3 ratio is 2.1

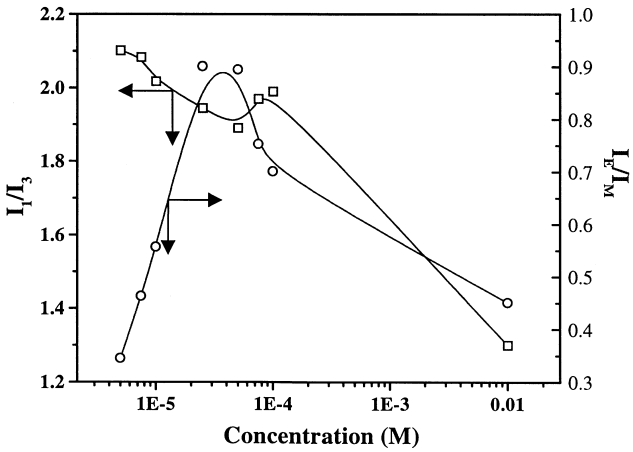

Figure 20. Pyrene fluorescence from a solution of didecyl monomer. (□) I_1/I_3 (○) I_EI_M [Pyrene] = $5x10^{-6}$ M.

for pyrene in water [48]. The I_1/I_3 values decrease with the addition of didecyl monomer. A local minimum in the plot is observed at approximately $5x10^{-5}$ M slightly above the CAC. In this range, the value of I_1/I_3 remains relatively high, suggesting a hydrated polar microdomain immediately around the pyrene molecule. Further increases in monomer concentration lead to a slight increase at $1x10^{-4}$M, followed by a sharp decline at 1×10^{-2} M to a value close to that reported for a compact polymer coil [47].

The ratio of the emission intensity of the pyrene fluorescence at a wavelength attributed to monomeric pyrene (383 nm) to that of dimeric pyrene (450 nm) has been used as a spectroscopic tool for studying the microdomains of species found in solution [48, 49]. The values of the I_E/I_M ratio calculated for the $C_{10}C_{10}$ monomer are also illustrated in Figure 20. The plot illustrates a maximum value of the I_E/I_M that occurs near the CAC of the didecyl monomer. At concentrations above the CAC, the value of the I_E/I_M decreases. This maximum in the I_E/I_M is attributed to the interaction of the pyrene with the surfactant aggregates in solution. At low concentrations below the CAC, the I_E/I_M increases due to the nucleation of small surfactant assemblies with the pyrene. As the concentration of surfactant increases, the number of sequestering domains increases, as well as the probability of two pyrene molecules occupying any one domain. At the CAC, this probability is the highest. Further addition of monomer creates a larger number of surfactant assemblies. As the number of domains increase, the probability of multiple pyrenes occupying a domain decreases. The pyrene fluorescence measurements support the results of the surface tension and dynamic light scattering experiments. The CAC determined in the fluorescence experiments occurs at the same concentration of diallyl monomer. Changes in the I_1/I_3 and the I_E/I_M are direct evidence of the hydrophobic nature of the surfactant domains.

Atomic Force Microscopy (AFM)

In order to further study the aggregates of the didecyl monomer, atomic force microscopy was performed. Solutions of the didecyl monomer of 0.01 g/dL (above the CAC) were prepared. Samples of the monomer solution were placed on freshly cleaved mica, then frozen and lyophilized. Imaging of the samples revealed well defined structures on the mica surface. Structures show a distribution of diameters with an average of approximately 150 nm (Figure 21). The size of these aggregates corresponds well with the dimensions observed with dynamic light scattering.

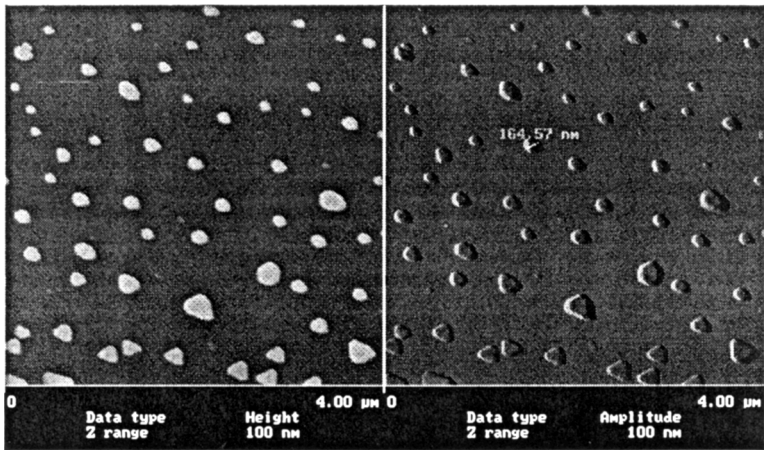

Figure 21. Atomic force microscopy image of $C_{10}C_{10}$ monomer on mica surface.

Nuclear Magnetic Resonance–Spin Lattice Relaxation Time (T_1)

Nuclear magnetic resonance provides an additional method for studying the aqueous solution properties of the monomer aggregates. The spin-lattice relaxation time (T_1) provides information about the local environment of a carbon nucleus. The spin lattice relaxation is a first order process represented by the relaxation time, T_1, which is a measure of the excited state lifetime of the nuclei. The T_1 is strongly affected by the mobility of the lattice [50]. In viscous systems or crystalline systems, where mobility is low, the value of the T_1 is large. As the mobility of a system increases, the number of vibrational and rotational frequencies increases, which enhances the probability of a magnetic fluctuation of the proper magnitude for a relaxation transition. As a consequence, the T_1 value is shorter. However, at very high mobilities, the number of rotational and vibrational frequencies in the system is so high, and they are spread over such a large range, the probability of suitable frequency for a relaxation decreases. As a result, the values may become larger [50].

Relaxation time measurements were made for each of the twin tail surfactants in aqueous solution. A ^{13}C spectrum of the didodecyl monomer and the measured T_1 values for each of the resonances at 2.5 wt% in aqueous solution are shown in Figure 22. A summary of the T_1 values for each of the monomers is listed in Table 3. The values for the relaxation times of the nuclei vary depend-

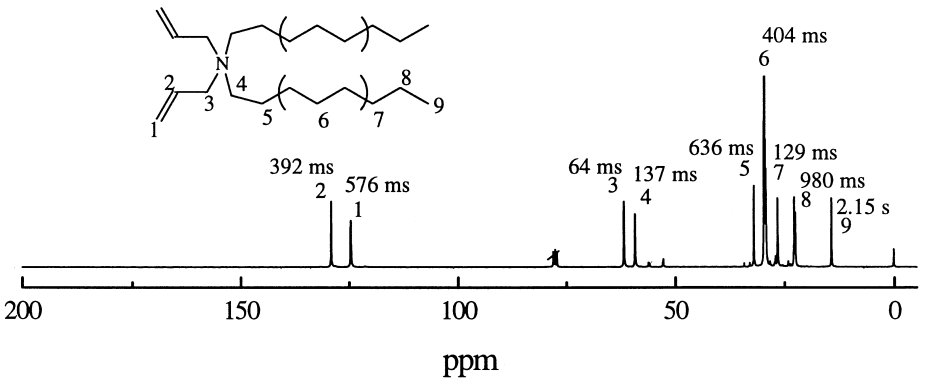

Figure 22. ^{13}C NMR spectrum of didodecyl monomer with spin-lattice (T_1) relaxation times determined for each resonance.

ing on the location of the carbon within the surfactant structure. The vinyl resonances of the monomer (1, 2), theoretically located at the charged headgroup region of the vesicle aggregates, have values of approximately 392 and 576 ms. The methyl carbons (3, 4) adjacent to the quaternary amine have shorter T_1 values of 64 and 137 ms. The methyl groups located at the end of the alkyl chains (9) have the longest relaxation times of over 2 seconds.

Comparison of the T_1 values of the twin tail monomers with values for other long chain surfactants and lipids provides insight into the local environment of the carbon nuclei. Previous work with 1-decanol has shown that the relaxation times of the carbon nuclei vary depending on the location of the respective carbons. Measurements of the T_1 for dihexadecanoyl phosphatidylcholine show a similar structure-dependent distribution. T_1 values for the carbons of each of these molecules are illustrated in Figure 23. The relaxation times

TABLE 3. T_1 Relaxation Time in Seconds of Carbon Resonances of Twin Tail Monomers in Aqueous Solution. [Monomer] = 2.5 wt%

	Resonance								
Monomer	2	1	3	4	5	6	7	8	9
C_8C_8	0.359	0.501	0.110	0.333	0.766	0.438	0.212	1.10	2.21
$C_{10}C_{10}$	0.375	0.895	0.200	0.347	1.18	0.687	0.399	1.60	2.37
$C_{12}C_{12}$	0.392	0.576	0.064	0.137	0.636	0.404	0.129	0.980	2.15

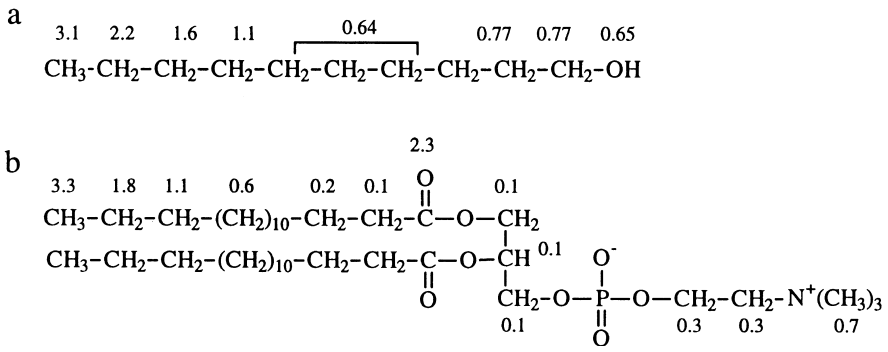

Figure 23. T_1 relaxation times in seconds for (a) 1-decanol and (b) dihexadecanoyl phosphatidylcholine in water.

measured for these two molecules increase along the alkyl chain length. In both cases, the variance in the T_1 values is attributed to differences in the mobility of the segments of the molecule. With 1-decanol, the five-fold increase in the T_1 values demonstrates that the terminal CH_3 moves much faster than the CH_2OH [50]. The decrease in the T_1 at the headgroup of the molecule is attributed to hydrogen bonding. The T_1 values observed with dihexadecanoyl phosphatidylcholine suggest that the structure is most tightly packed at the glycerol group. The molecular motions of the carbons in the fatty acid chains increase toward the methyl groups at the terminal chain end.

The distribution of the relaxation times of these structurally similar molecules corresponds well with the values calculated for the twin tail surfactants synthesized in this work. In all these materials, a long relaxation time is indicative of high mobility. Short relaxation times reflect low mobility. These results suggest that the headgroup region of the twin tail monomers is tightly packed in the vesicular assembly. The T_1 values for the alkyl chains suggest a high degree of mobility and fluidity within the hydrophobic domains of the aggregate.

Deuterium NMR

Deuterium NMR experiments were performed with each of the monomers to study the phase behavior at higher concentrations. This technique has been used to characterize phases and to study the water binding to the polar headgroups of surfactant molecules in liquid crystalline phases [33, 51, 52]. The deuteron nucleus has a spin quantum number of 1 and an electric quadrupole moment. The NMR spectrum of deuterium is dominated by the interaction of the

quadrupole moment with the electric field gradients at the nucleus. If the deuterium is in an anisotropic environment, this interaction generates a spectrum with two peaks. The distance between the peaks is the quadrupole splitting (Δ). The presence of the split signal and the value of the quadrupole splitting are indicators of the phase of the system. In an isotropic phase, such as a micelle or cubic phase, a single sharp singlet is observed. In an anisotropic phase, such as a lamellar or hexagonal phase, the quadrupole splitting is observed.

Deuterium NMR experiments were performed to investigate the presence of liquid crystalline phases at high monomer concentrations (5-95 wt%). For the C_8 and C_{10} twin tail monomers, a sharp singlet was observed at all concentrations. Experiments with the twin $C_{12}C_{12}$ monomer showed a quadrupole splitting indicative of an anisotropic environment. The effect of monomer concentration on the deuterium spectrum with the twin $C_{12}C_{12}$ monomer is illustrated in Figure 24. At concentrations greater than 6 wt%, quadrupolar splitting was observed. The figure illustrates an increase in the quadrupolar splitting with an increase in the monomer concentration.

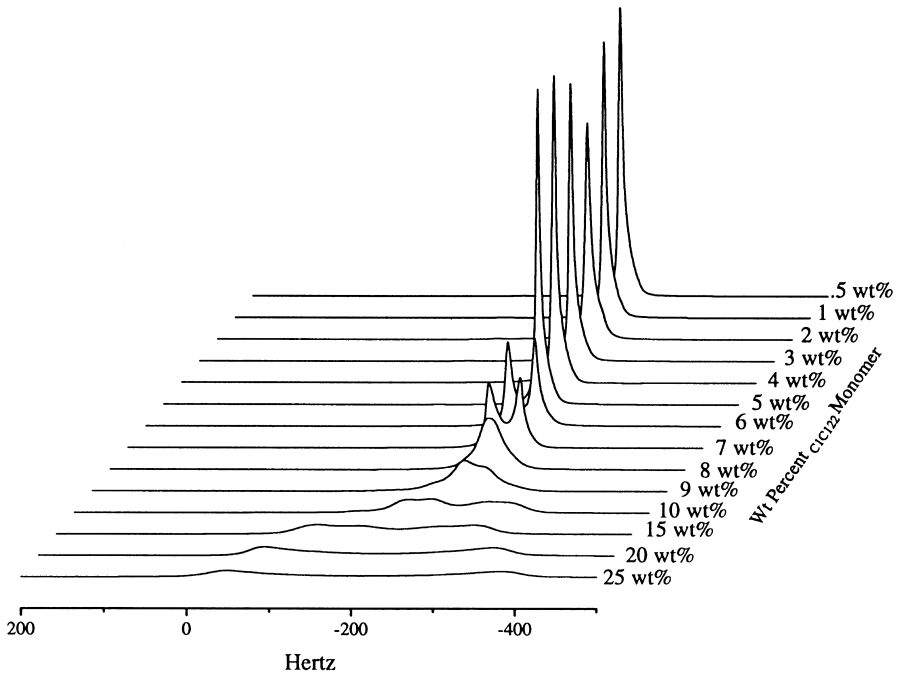

Figure 24. Deuterium NMR signal of D_2O as a function of $C_{12}C_{12}$ monomer concentration. T=25°C.

Changes in the value of the quadrupole splitting with concentration of water in the sample have been used to study the interaction of water with the headgroup of the surfactant [33]. In order to rationalize the values of the quadrupolar splitting, a two site model may be used [53]. In this case, there are two types of water molecules; 'free' and 'bound'. The bound water represents the water molecules associated with the ionic headgroup of the surfactant. The free water represents the fraction of water that is not bound by the ionic headgroup and populates the spaces between the ordered surfactant assemblies. The splitting may be expressed as a function of the mole ratio between surfactant and water [33].

$$\Delta = nV_Q S\left(\frac{(1-X_w)}{X_w}\right) \tag{IV-5}$$

Where X is the mole fraction of water in the sample; *n* is the average number of hydrating water molecules per surfactant molecule. S is the order parameter and V_Q is the deuterium quadrupole coupling constant (~220 kHz) [54]. Assuming *n* and S are constants, for the compositions studied in this work,

$$\Delta = k_1\left(\frac{(1-X_w)}{X_w}\right) \tag{IV-6}$$

a plot of Δ vs $(1-X_w)/X_w$ yields a straight line through the origin where the hydration properties of the surfactant are independent of water content [33]. In systems of this type, any increase in the water content has been shown to affect only the amount of free water that is non-associated with the monomer [32]. Shown in Figure 25 is the observed quadrupole splitting, Δ, as a function of the mole ratio. The data were fit to a straight line passing close to the origin. The parameters determined from this plot are identical to those calculated for the model compound DDAC [33]. For both of these surfactants, water acts to swell the intralamellar spacings and the hydration of the surfactant headgroups is independent of the water content.

Further experiments with the C_{12} twin tail monomer were performed to study the temperature sensitivity of the liquid crystalline phase. The change in the deuterium spectrum as a function of temperature is illustrated in Figure 26. Initially, the sample of the C_{12} monomer was observed to exhibit a broad signal with quadrupolar splitting of 750 Hz at 25°C. As the temperature was increased to 35°C, the quadrupolar splitting was observed to decrease and a single sharp peak was observed. Further increases in the temperature led to a complete loss

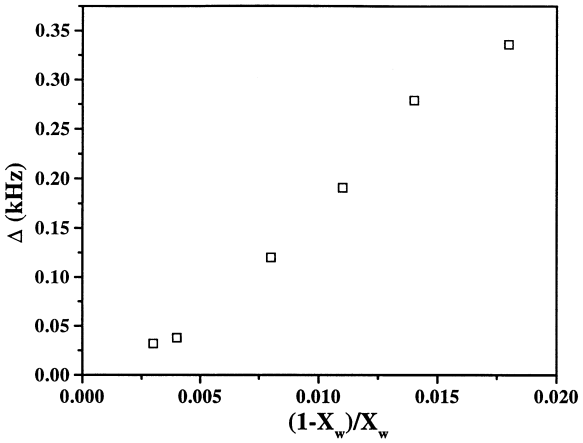

Figure 25. Deuterium quadrupolar splitting measured in the liquid crystalline phase with didodecyl monomer at 25°C.

of the quadrupolar splitting and at 55°C, only a single peak was observed. This change in the spectrum indicated a loss of the anisotropic properties of the sample at elevated temperatures. Cooling of the sample from 55°C to 45°C led to the appearance of two sharp peaks in addition to the isotropic peak. Further cooling to 25°C led to a complete loss of the singlet and an evolution of two well resolved peaks with the same quadrupolar splitting value as that of the freshly prepared sample at 25°C. This heating and cooling process appears to have enhanced the ordering of the lamellar phase.

Polarizing Microscopy

The liquid crystalline properties of the C_{12} twin tail monomer at high concentrations were studied by polarizing microscopy. This technique has been widely used to determine the nature of liquid crystalline materials [55]. Anisotropic and liquid crystalline phases are birefringent when observed between crossed polarizers. The resulting birefringent textures are used to characterize the liquid crystalline phase. Isotropic or cubic phases appear as a dark background in the polarizing microscope. Lamellar phases have a mosaic planar texture and hexagonal structures show fanlike angular or nongeometric pattern texture [56].

Polarizing microscopy images of the C_8 and C_{10} monomer show no birefringence across the concentration range of 5-95 wt%. The C_{12} twin tail

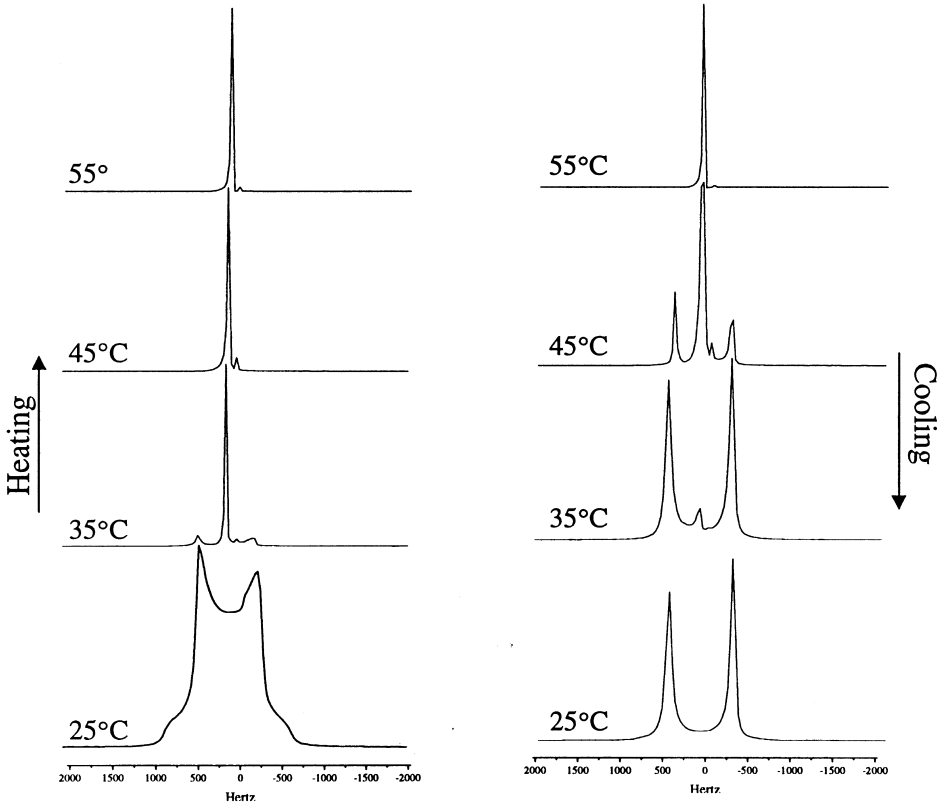

Figure 26. Effect of heating and cooling cycles on the observed deuterium NMR spectrum of $C_{12}C_{12}$ monomer. [Monomer] = 75 wt%.

monomer, however exhibits birefringent patterns at concentrations above 10 wt%. An image of the birefringent structures of the C_{12} twin tail monomer at 50 wt% is illustrated in Figure 27. Throughout the image, small maltese cross patterns were observed along with mosaic structures. Both of these types of patterns have been attributed to lamellar phases [33]. The birefringent structures formed by the monomer correspond well with previous images of a lamellar phase formed by didodecyl dimethyl ammonium bromide (DDAB) [34]. The birefringent liquid crystalline phase was found to change with temperature. A slow temperature increase from 25°C to 55°C caused a gradual loss of the birefringent structures. At 55°C, the sample was observed to be completely dark, indicating the presence of an isotropic phase.

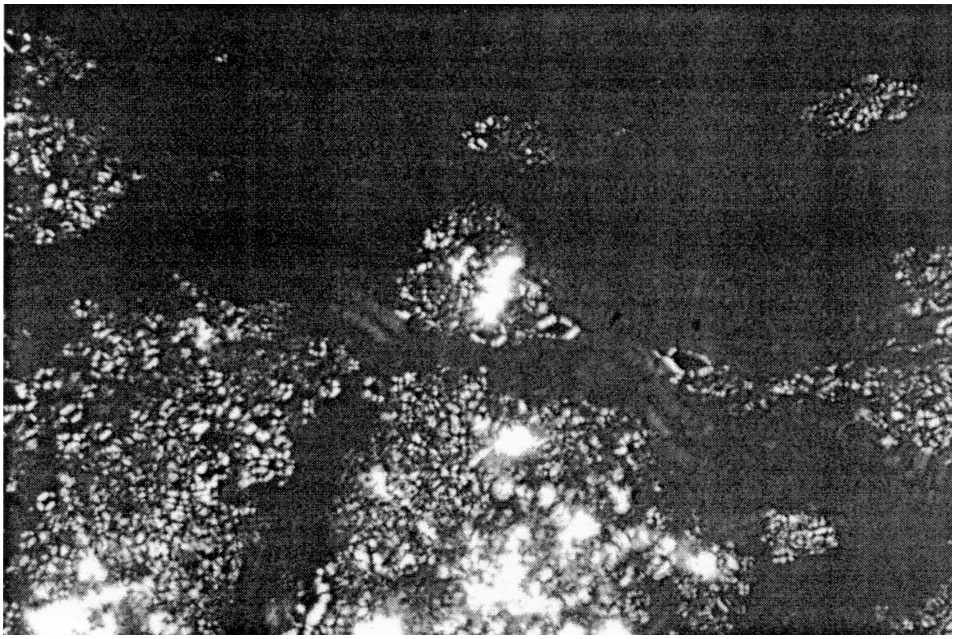

Figure 27. Optical micrographs of the didocecyl monomer/H_2O System at 25°C. (Monomer = 50 wt%).

Small Angle X-Ray Scattering (SAXS)

Small angle X-Ray scattering experiments were performed with the C_{12} twin tail monomer to investigate the properties of the liquid crystalline domains present at high monomer concentrations. X-Ray scattering has been widely used as a tool to characterize the phases of liquid crystalline materials [57]. The scattering pattern of an amphipathic liquid crystal is characterized by a series of sharp reflections corresponding to interplanar spacings. Structures with one dimensional periodicity such as a lamellar phase usually show reflections with d-spacings in the ratio of 1:1/2:1/3:1/4. However, in aqueous systems, the intensities of the higher ordered reflections fall off sharply and often only the first peak is visible. Other phases such as those with hexagonal periodicity and the square phase have also been characterized and found to have unique ratios of the d-spacings.

Measurements of the low angle X-ray spacing intensities were recorded at 25°C. The scattering pattern observed for the $C_{12}C_{12}$ monomer at 30 wt%

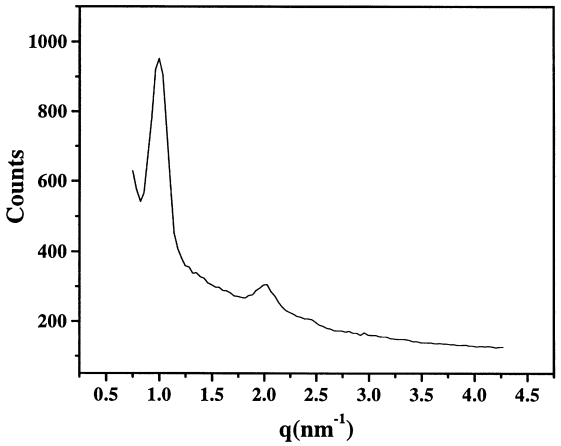

Figure 28. Small angle X-ray scattering from $C_{12}C_{12}$ monomer in water. [Monomer] =30 wt%. T = 25°C.

monomer is illustrated in Figure 28. Calculations of the d-spacings for the monomer have the ratio of 1:1/2, a value found for lamellar phases. The ratio of the d-spacing was calculated for samples of monomer of varying weight percent. For each sample from 30 to 70 weight percent, the ratios of the d-spacing was observed to remain 1:1/2. While the d-spacings remained constant with a change in the water content, the position of each peak shifted in relation to the amount of water present. As the water content was decreased, the values indicated lower d-spacings.

Studies of the aqueous solution properties show that the twin tail monomers behave much like other small molecule surfactants. In particular, the twin tail C_{12} monomer exhibits liquid crystalline ordering at high concentrations. At dilute concentrations, the monomer forms organized spherical vesicles. The presence of well organized, stable domains presents an opportunity to investigate the influence of liquid crystalline order on the sequestration of *p*-cresol. Information from these studies might be expected to provide insight into binding efficiency in highly ordered domains.

Equilibrium Dialysis

Equilibrium dialysis experiments were performed with the C_{12} twin tail monomer at a concentration of 0.1 M. At this concentration, the monomer forms large, stable structures in aqueous solution. Temperature was varied to observe

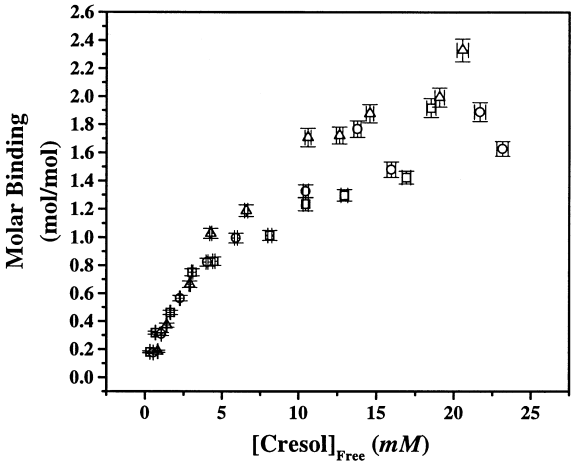

Figure 29. Binding isotherms for $C_{12}C_{12}$ monomer as a function of cresol as a function of temperature. (□) 5°C, (O) 25° and (Δ) 45°C. [Monomer] = 0.1 M.

any changes in the sequestration of cresol through an increase in the fluidity of the aliphatic chains of the surfactant assembly. The binding isotherms for the C_{12} monomer at 5°C, 25°C, and 45°C are illustrated in Figure 29. The binding isotherms for the C_{12} are similar at low free cresol concentrations. The molar binding increases with the addition of *p*-cresol at each of the temperatures. At higher concentrations of cresol (>10mM), slight differences in the molar binding are observed. The monomer at 45°C has higher binding values than those measured at 25°C and 5°C, respectively. The higher molar binding observed at 45°C is expected and is consistent with previous research indicating the importance of chain fluidity on the ability of the hydrophobic materials to penetrate and reside within hydrophobic domains [57, 58].

The rejection ratios and activity coefficients were determined from the dialysis experiments and are listed in Table 4. The activity coefficients and rejection ratios for the twin tailed monomer provide insight into the interaction of the monomer with cresol. At each temperature, the values of the activity coefficient reflect a strong interaction between the cresol and the monomer aggregates. As the amount of cresol present in the domains increases, the value of the activity coefficient increases indicating a change in the properties of the surfactant aggregate. At the higher concentrations of cresol (48-70 mM), the mole fraction of the

TABLE 4. Rejection Ratios for $C_{12}C_{12}$ Monomer as a Function of Temperature. ($C_{monomer}$ = 0.1 M)

	$[C_{12}C_{12}]$ = 0.1 M T = 5°C		$[C_{12}C_{12}]$ = 0.1 M T = 25°C		$[C_{12}C_{12}]$ = 0.1 M T = 45°C	
$[Cresol]_{feed}$ (mM)	Rejection Ratio (%)	Activity Coefficient	Rejection Ratio (%)	Activity Coefficient	Rejection Ratio (%)	Activity Coefficient
4	92±3	0.01	87±3	0.02	82±3	0.03
8	91±3	0.01	86±3	0.03	85±3	0.03
16	86±2	0.03	84±3	0.04	83±3	0.04
24	84±3	0.03	81±3	0.05	83±3	0.05
32	80±2	0.05	73±2	0.10	79±3	0.07
48	72±2	0.09	78±3	0.06	77±3	0.09
56	71±2	0.10	66±2	0.14	74±2	0.11
64	68±2	0.12	73±2	0.12	73±2	0.12
72	64±2	0.16	60±2	0.20	69±2	0.16
80	68±2	0.15	65±2	0.18	70±2	0.16

cresol within the domains approaches 0.7 (data not shown). Such high concentrations of cresol most likely lead to the formation of assemblies of monomer and cresol similar to mixed micelles.

CONCLUSION

A series of single and twin tail polymerizable surfactants based on diallylammonium salts have been synthesized. These synthetic monomers are surface active as demonstrated by surface tensiometry. The single tail monomers represent pH responsive materials that may be used for the development of hydrophobically modified polymers and copolymers. The twin tail monomers form large, ordered assemblies at dilute concentrations as indicated by light scattering, fluorescence and NMR experiments. Investigations of higher concentrations of the twin tailed C_{12} monomers indicate a lyotropic lamellar liquid crystalline phase in the concentration range of 10-75 wt%. The ordering of the phase is temperature dependent.

The dispersed lamellar vesicles of the C_{12} twin tailed monomer have a high affinity for *p*-cresol in equilibrium dialysis experiments. With higher amounts of cresol present in the surfactant assembly, the properties of the

domains change significantly, indicating the formation of mixed micellar aggregates. The large monomer assemblies are retained by the dialysis membrane and present an attractive alternative to small micellar assemblies. These vesicle assemblies appear to be well suited for the sequestration of a number of different hydrophobic species. The domains encompass a large hydrophobic volume that would be useful for sequestration in micellar enhanced ultrafiltration applications. The domains also have a very high polar volume due to the multilamellar bilayer structure that would foster the binding of large numbers of polar amphipathic materials.

ACKNOWLEDGEMENTS

Support for this research by the Office of Naval Research and the Department of Energy is gratefully acknowledged.

REFERENCES

[1] S. L. Regen, B. Czech, and A. Singh, *J. Am. Chem. Soc., 102*, 6639 (1980).

[2] S. L. Regen, K. Yamaguchi, N. K. P. Samuel, and M. Singh, *J. Am. Chem. Soc., 105*, 6354 (1980).

[3] D. Bolical and S. L. Regen, *Macromolecules, 17*, 1287 (1984).

[4] H. H. Hub, B. K. Hupfer, K. Korst, and H. Ringsdorf, *Angew. Chem., Int. Ed. Engl., 19*, 938 (1980).

[5] K. Dorn, R. T. Klingbel, D. P. Spect, P. N. Tyminski, H. Ringsdorf, and D. F. O'Brien, *J. Am. Chem. Soc., 106*, 1627 (1984).

[6] H. Koch and H. Ringsdorf, *Makromol. Chem., Rapid Commun., 1*, 255 (1980).

[7] B. Hupfer, H. Ringsdorf, and H. Schupp, *Makromol. Chem., 182*, 247 (1981).

[8] A. Akimoto, K. Dorn, L. Gros, H. Ringsdorf, and H. Schupp, *Angew. Chem., Int. Ed. Engl., 20*, 90 (1981).

[9] H. Bader, H. Ringsdorf, and J. Skura, *Angew. Chem., Int. Ed. Engl., 20*, 90 (1981).

[10] M. Gratzel, *Ber. Bunsenges. Phys. Chem., 84*, 981 (1980).

[11] K. I. Zamaraev and V. N. Parmon, *Russ. Chem. Rev., 52*, 1433 (1983).
[12] M. Kaneko and A. Yamada, *Adv. Polym. Sci., 55*, 2 (1984).
[13] J. H. Fendler, *J. Phys. Chem., 89*, 2730 (1985).
[14] J. F. Rabek, *Prog. Polym. Sci., 13*, 83 (1988).
[15] B. E. Ryman and D. A. Tirrell, in *Essays in Biochemistry*, P.N. Campell and R. D. Marshall, Eds., Academic, New York, 1981, p. 49.
[16] D. A. Tirrell, L. G. Donamura, and A. B. Turek, in *Macromolecules as Drugs and as Carriers for Biologically Active Materials*, Ann. N.Y. Acad. Sci., New York, 1985, p. 446.
[17] Y. Kondo, M. Abe, K. Ogino, H. Uchiyama, J. F. Scamehorn, E. E. Tucker, and S. D. Christian, *Langmuir, 9*, 899 (1993).
[18] M. Hebrant, P. Tecilla, P. Scrimin, and C. Tondre, *Langmuir, 13*, 5539 (1997).
[19] P. Tounissou, M. Hebrant, L. Rodeheuser, and C. J. Tondre, *Colloid Interface Sci., 183*, 484 (1996).
[20] S. W. Provencher, *Comput. Phys. Commun., 27*, 229 (1982).
[21] A. Goto and F. Endo, *J. Coll. Interf. Sci., 66*, 26 (1978).
[22] P. Mukerjee and J. R. Cardinal, J. Phys. Chem., 82, 1620 (1978).
[23] D. W. Armstrong and F. Nome, *Anal. Chem., 53*, 1662 (1981).
[24] M. Arunyanart and L. J. Cline-Love, *Anal. Chem., 56*, 1557 (1984).
[25] C. Treiner and A. K. Chattopadhuay, *J. Coll. Interf. Sci., 98*, 447 (1984).
[26] J. Sepulveda, E. Lissi, and F. Quina, *Adv. Coll. Interf. Sci., 25*, 1 (1986).
[27] A. Malliaris, *Adv. Coll. Interf. Sci., 27*, 153 (1987).
[28] B-H. Lee, S. D. Christian, E. E. Tucker, and J. F. Scamehorn*, Langmuir, 16*, 230 (1990).
[29] S. D. Christian, E. E. Tucker, J. F. Scamehorn, and H. Uchiyama*, Coll. and Polym. Sci., 271*, 745 (1994).
[30] S. N. Bhat, G. A. Smith, E. E. Tucker, S. D. Christian, J. F. Scamehorn, and W. Smith, *Ind. Eng. Chem. Res., 26*, 1217 (1987).
[31] G. G. Warr, D. Radha Sen, and F. Evans, *J. Phys. Chem., 92*, 774 (1988).
[32] Y. J. Uang, F. D. Blum, S. E. Friberg, and J. F. Wang, *Langmuir, 8*, 1487 (1992).
[33] C. Kang and A. Khan, *J. Coll. and Interf. Sci., 156*, 218 (1993).
[34] F. Caboi and M. Monduzzi, *Langmuir, 12*, 3548 (1996).
[35] O. Regev and A. Khan, *Progr. Coll. Polym. Sci., 97*, 298 (1994).
[36] K. Fontell and M. Jansson, Progr. Coll. Polym. Sci., 76, 169 (1988).

[37] S. J. Chen, D. F. Evans, B. W. Ninham, D. J. Mitchell, F. D. Blum, and S. Pickup, *J. Phys. Chem., 90*, 842 (1986).
[38] H. Kunieda and K. Shinoda, *J. Phys. Chem., 82*, 1710 (1978).
[39] M. Dubois and T. Zemb, *Langmuir, 7*, 1352 (1991).
[40] T. Zemb, D. Gazeau, M. Dubois, and T. Gulik-Krzywicki, *Europhys. Lett., 21*, 7 59 (1993).
[41] J. N. Israelachvili, D. J. Mitchell, and B. W. Ninham, *J. Chem. Soc. Faraday Trans. 2, 72*, 1525 (1976).
[42] H. Wennerström and B. Lindmann, *Phys. Rep., 52*, 1 (1979).
[43] D. J. Mitchell and B. W. Ninham, *J. Chem. Soc. Faraday Trans. 2, 77,* 609 (1981).
[44] A. Caria, O. Regev, and A. Khan, *J. Coll. Interf. Sci., 200*, 19 (1998).
[45] D. Shaw, in *Introduction to Colloid and Surface Chemistry,* Butterworths, London, 1970.
[46] K. Kalyanasundaram, *Langmuir, 4*, 842 (1988).
[47] Y. Chang and C. L. McCormick, *Polymer, 35*, 3503 (1994).
[48] K. D. Branham, G. S. Shafer, C. E. Hoyle, and C. L. McCormick*, Macromolecules, 25*, 6175 (1995).
[49] K. Prochazka, T. J. Martin, P. Munk, and S. E. Webber*, Macromolecules, 29*, 6581 (1996).
[50] Y. K. Levine, N. J. M. Birdsall, A .G. Lee, and J. C. Metcalf, *Biochemistry, 11*, 1416 (1982).
[51] A. Khan, K. Fontell, G. Lindblom, and B. Lindman, *J. Phys. Chem., 86*, 4266 (1982).
[52] J. Ulmius, H. Wennerström, G. Lindblom, and G. Arvidson, *Biochemistry, 16*, 5742 (1977).
[53] H. Wennerström, N. O. Persson, and B. Lindman, *Am. Chem. Soc. Symp. Ser., 9*, 253 (1975).
[54] J. A. Glasel, in *Water, A Comprehensive Treatise*, F. Franks, Ed., Plenum Press, New York, New York, 1972, p. 215.
[55] N. H. Hartshorne, in *Liquid Crystals and Plastic Crystals*, G. W. Gray, P. A. Winsor, Eds., John Wiley and Sons, New York, NY, 1974, p. 24.
[56] F. B. Rosevear, *J. Soc. Cosmet. Chem., 19*, 581 (1968).
[57] M. Abe, K. Ogino, and H. Yamauchi, in *Separation Science Review*, J. Scamehorn, S. E. Christian, Eds., Plenum Press, New York, NY, 1992, p. 333.

[58] M. Hebrant, P. Techilla, P. Scrimin, and C. Tondre, *Langmuir, 13*, 5539 (1997).

[59] C. Tanford, in *The Hydrophobic Effect: The Formation of Micelles and Biological Membranes*, John Wiley and Sons, New York, NY, 1980.

[60] D. W. R. Gruen, *J. Phys. Chem., 89*, 146 (1985).

Received February 26, 1999